Preparation of multilayer microcapsules encapsulating aqueous lithium bromide and their mechanical stability

Iqbal, Parvez; Lu, Tiejun; Zhang, Zhibing; Li, Yongliang

DOI:
10.1021/acs.iecr.8b02782

Preparation of Multilayer Microcapsules Encapsulating Aqueous Lithium Bromide and Their Mechanical Stability

Journal:	*Industrial & Engineering Chemistry Research*
Manuscript ID	ie-2018-027826.R2
Manuscript Type:	Article
Date Submitted by the Author:	25-Jan-2019
Complete List of Authors:	Iqbal, Parvez; University of Birmingham, School of Chemical Engineering Lu, Tiejun; University of Birmingham, Chemical Engineering Zhang, Zhibing; University of Birmingham, School of Chemical Engineering Li, Yongliang; University of Birmingham, School of Chemical Engineering

Preparation of Multilayer Microcapsules Encapsulating Aqueous Lithium Bromide and Their Mechanical Stability

Parvez Iqbal, Tiejun Lu, Zhibing Zhang and Yongliang Li

School of Chemical Engineering, University of Birmingham, Edgbaston, Birmingham B15 2TT, UK

Corresponding authors:

Dr Yiongliang Li

School of Chemical Engineering,

University of Birmingham,

Edgbaston,

Birmingham,

B15 2TT,

UK

Tel No: 0121 414 5135

E-mail: *y.li.1@bham.ac.uk*

Prof Zhibing Zhang

School of Chemical Engineering,

University of Birmingham,

Edgbaston,

Birmingham,

B15 2TT,

UK

Tel No: 0121 414 5324

Email: z.zhang@bham.ac.uk

Abstract

The development of more efficient and reliable absorption/adsorption refrigeration for air conditioners (ACs) and chillers is of great interest due to the increasing demand of these cooling devices in homes and offices. Presently, majority of the ACs incorporate aqueous lithium salts as both refrigerate and desiccant, which are corrosive and lead to corrosion of the mechanical components. This increases maintenance costs and decreases the cooling system's lifespan. Herein, an encapsulation method is proposed to encompass the aqueous lithium bromide solution with silica as the shell to protect the surrounding mechanical components. Moreover, a coating of citrate stabilised Au nanoparticles via an electroless method involving intermolecular electrostatic interactions is introduced to improve the robustness of the capsule wall. The success of the different coatings is evident from the change of zeta potential and mechanical properties. The coating with Au nanoparticles improves the mechanical strength of the capsules significantly, increasing rupture force from 0.25 ± 0.02 mN to 0.45 ± 0.04 mN. The coated and uncoated capsules were shown to be thermally stable over 10 repeated cycles between temperature ranges -10 to 150 ^{o}C, hence, withstand the thermal demands in ACs. Furthermore, adsorption and desorption cycles were performed on the capsules, which showed promising stable and repeatable performances.

Keywords. Microencapsulation, Lithium bromide, Electroless coating, Multilayer capsules, Rupture force.

1.0 Introduction

Lithium halides (bromide and chloride) have been widely used in variety of applications which include medicinal[1-3] and organic synthesis.[4-7] In medicine, lithium halides especially lithium bromide (LiBr) have previously been used in clinical psychopharmacology as a hypnotic drug in the late nineteenth and early twentieth century.[1-3] In addition, LiBr was one of the first compounds regularly employed as an antianxiety agent.[3] Whereas, in organic synthesis, lithium halides have been often employed as a catalyst[4] or as a lewis acid[5] or as a source of bromine in nucleophilic substitution[6] and addition reactions.[7] Recently, LiCl and LiBr as the consequences of their highly hydroscopic properties[8,9] have been increasingly used as desiccants for absorption cooling systems such as air conditioners (ACs) for the utilisation and conversion of low grade waste heat and renewable energy.[10-12]

In a typical adsorption AC, water is often used as the refrigerant and lithium salt (either chloride or bromide) as the desiccant.[10-12] The system operates via two loops: one containing the refrigerant and the other desiccant. In simple terms, the gaseous water vapours are introduced to contact the concentrated lithium salt solution; when the two come in contact, the water vapour is absorbed by the salt solution, which was hence diluted. The original concentrated lithium salt solution is then regenerated through the evaporation of the water and the cycle repeats itself. One of the major benefits of such system in respect to the more commonly used vapour compression cooling energy system is that the process is less energy intensive and hence, can be run by lower-grade energy such as waste energy or solar power.[10-12] Furthermore, the system is less noisy, more reliable, requires low maintenance and there is no environmentally harmful chemical used as the refrigerant. However, there is a major drawback restricting the usage and lifespan for such systems, which is a direct consequence of the corrosive properties of the lithium salts. Hence, there is a risk of parts corroding via exposure to the salts which subsequently leads to hazardous leaks. Moreover, there is also a risk of lithium salt crystallizing from the solution leading to the system becoming less efficient.[13] It is apparent that to improve the lifespan and efficiency of such systems the lithium salt solutions need to be concealed from the surrounding mechanical components. A possible approach could be to encapsulate the lithium salts in such a way that water can be absorbed and released selectively without the lithium salt being released. Furthermore, in recent studies it has been demonstrated that microencapsulated sorbents exhibit an order-of-magnitude higher sorption rate relative to neat sorbents of equivalent mass,[14] hence this may provide further additional benefit for encapsulating lithium salt solution.

Encapsulation is a process which involves the entrapment of tiny particles or droplets within a coating of polymer[15-17] or inorganic material,[18] which is commonly used in medicine, textile, veterinary, chemical industry, biotech, food and electronics.[15-17] The list is growing, as different industries try to reap the ample benefits of encapsulation which include increasing shelf life, enhanced properties, improving stability, slow release, delay release, masking taste and odours.[15-17] Moreover, by tuning the chemical and physical parameters of the capsules. They can be adapted to meet different requirements of the applications such as controlled release rate[19] and encapsulation of phase change material for long-term use.[20,21]

To develop capsules which encapsulate aqueous lithium bromide solution and possess the desired properties such as having robust and semi-permeable walls so that the water vapour molecules can exit and enter back into the capsules without the capsules rupturing due to the changes in pressure and temperature. Moreover and most importantly the capsules should eliminate/minimise the loss of LiBr from the core during the thermal cycles, otherwise the system will become less efficient and water ingress is likely to happen to replace the loss of LiBr, leading to changes in the physical environment within the capsules such as internal pressure. Hence, a 'hybrid' approach will be used which incorporates both polymer and metallic materials to form the capsule wall so that the capsules can benefit from the properties associated with both coating materials.[10,22-24] The polymer material will hopefully provide the required semi-permeability properties to enable the water vapours to escape and re-enter the capsules,[22,23] whereas the metallic material will enhance the robustness and thermal properties of the capsule wall.[21,24] Herein, LiBr will be used as the adsorbent instead of LiCl as previous studies have shown that although LiCl has stronger affinity to water compared to LiBr, it has shorter life span than LiBr.[25] Additionally, it has been shown that the more concentrated the LiBr solution the more effective it is as an absorbent.[26] Hence, as the solubility of LiBr at 25 °C is 62 % (w/w) in water, the saturated aqueous solution of LiBr will be used. Silica will be used as the main coating material, not only because it will provide a robust and semi-permeable wall,[21] it will also most importantly, provide a surface which can be further chemically manipulated to fine tune the surface properties.[27-30]

Scheme 1 shows the strategy proposed for the incorporation of both polymer and metallic material in the capsule wall. The strategy involves firstly encapsulation of aqueous solution of lithium bromide (LiBr) via in-situ polymerisation method using silica as coating material followed by functionalisation of the capsule wall with amine via reacting the surface with 3-

aminotrimethoxysilane (APTMS) to enable attachment of Au (as a model of metallic material to prove the feasibility) nanoparticles onto the polymer coating through physical interaction. It is well documented that the amine functionalised surface has affinity to negative charged particles such as citrate stabilised Au nanoparticles and optimum binding between these Au nanoparticles and amine functionalised surfaces are observed in the range pH 4.5-5.[29,30] Finally, the capsules will be coated with organic polymer to ensure the nanoparticles remain bound to the shell. Furthermore, to evaluate the suitability of the capsules for the intended application as composite materials for cooling systems, the mechanical and thermal stabilities of the formed capsules will be investigated prior to and after exposure to repeated thermal cycles over the temperature range -10 °C to 150 °C for each coating as well as the encapsulation efficiency (EE) and active load will be determined to investigate the efficiency of the formulation process.

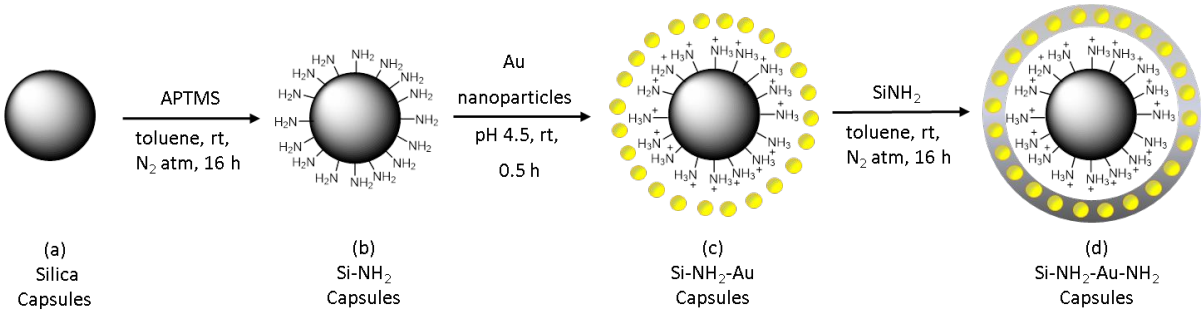

Scheme 1. Schematic representation of strategy for encapsulation of LiBr aqueous solution; (a) formation capsule through use of polymer material as primary capsule wall, (b) functionalisation of the capsule wall, in this case with amine moieties via reaction with APTMS, (c) Depositing of Au nanoparticles onto the primary shell wall and (d) second polymer wall to covalently bind the Au nanoparticles onto the capsule wall.

2.0 Results and discussion

2.1 Preparation of microcapsules

Encapsulation via in-situ polymerisation was performed under acidic conditions at elevated temperature (Scheme 1) using precondensate formed from a mixture of tetraethoxysilane (TEOS) and methyl trimethoxysilane (MMTS). The MMTS was added to prevent the agglomeration of the capsules via hindering the intermolecular hydrogen bonding between the hydroxyl moieties on adjacent capsules. Further functionalisation of the capsule wall was carried out under inert atmosphere and ambient temperature in the presence of the monomer 3-aminopropyltrimetoxysilane (APTMS). Citrate functionalised Au nanoparticles (see Figure S1 in

Electronic Supplementary Information (ESI) for characterisation of the Au nanoparticles) were deposited onto the capsule walls under mild acidic conditions (pH 4.5) to ensure optimal condition for electrostatic binding between the positive charged protonated amine (-RNH_3^+) and negative charged carboxylates (-$RCOO^-$) as previously reported.[29,30] Finally, a coating of polymer formed from APTMS was deposited onto the Au layer under inert atmosphere and ambient temperature.

2.2 Capsule characterisation

The capsules were characterised using Dynamic Light Scatter (DLS), Scanning Electron Microscopy (SEM) and Flame Photometer. First and foremost the sizes of the microcapsules were measured using DLS and capsule morphology was observed via SEM and optical microscope.

From SEM images (Figure 1a) the capsules formed are shown to be quasi spherical particles. The surface morphology after the APTMS coating remains similar to prior the coating as evident in Figure 1b. However, after the coating of Au nanoparticles it seems there are white lumps of particulates on the capsule surface (Figure 1c), they are obviously too large to be individual nanoparticles, hence these are likely to be Au nanoparticle aggregates which have settled on the surface. Finally, compared to $SiNH_2$-Au capsules (1c), the outermost coating of the APTMS shows no immediate change in the surface morphology (1d). The white Au particle lumps are still clearly present (Figure 1d) and a close-up SEM image of the $SiNH_2$-Au-NH_2 microcapsules surface clearly shows the presence of Au-nanoparticles (Figure 2b). Figure 2 shows zoom-in SEM images of $SiNH_2$-Au and $SiNH_2$-Au-NH_2 microcapsule surface, and indicate the nanoparticles are well distributed on the surface and most importantly, not completely covering the surface so that there may be minimal effect on the semi-permeable properties of the capsules. The Au nanoparticle surface coverage on the capsules is calculated as 28 ± 3 % which equals 381,680 particles on each capsule (see ESI for more details on how the au nanoparticle surface coverage was determined).

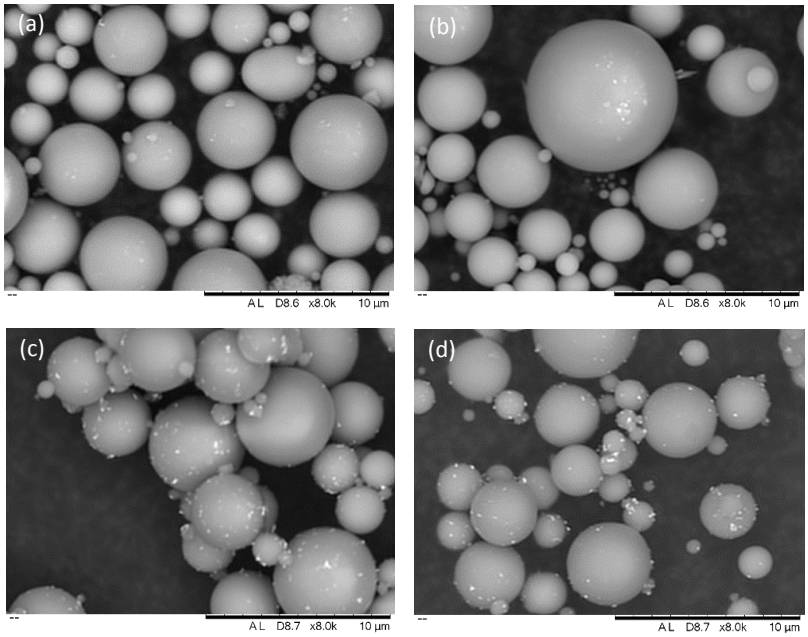

Figure 1. SEM images of (a) Silica, (b) $SiNH_2$ (c) $SiNH_2$-Au and (d) $SiNH_2$-Au-NH_2 microcapsules.

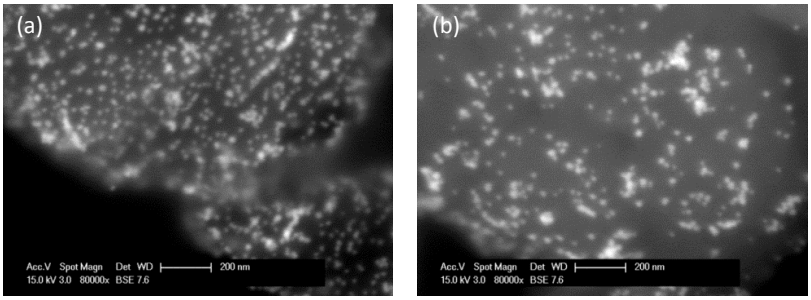

Figure 2. SEM zoom in image of (a) $SiNH_2$-Au capsule and (b) $SiNH_2$-Au-NH_2 capsule showing the distribution of the particles.

The size distribution of the capsules in all the samples is large between 2-50 µm (see ESI, Figure S2). The average silica capsule size observed via DLS was shown to be 8.3 µm with coefficient variance (CV) of 0.5 (see Table 1 and Figure S3 in ESI for the size distribution). Both the average size and CV increase with each coating with final size observed for Si-NH_2-Au-NH_2 capsules as 9.2 µm with CV of 0.7. An increase in mean size of 0.9 µm is observed between the initial silica capsules and final coating of polymer. This observed increase in capsule size suggests that there is a growth on the

capsule walls after each coating. Furthermore, an increase in mean shell thickness is observed after each coating of the capsules from 1.1 ± 0.2 to 1.5 ± 0.4 μm.

2.3 Encapsulation efficiency and active load

The encapsulation efficiency (EE) and active load were determined by crushing known mass of capsules followed by determining the amount of Li^+ ions released using a flame photometer. Equation 1 and 2 were used to determine the EE and active load, respectively.

$$EE = \frac{\text{Amount of LiBr encapsulated}}{\text{Total amount LiBr used}} \times 100 \quad (1)$$

$$\text{Active load (AL)} = \frac{\text{Amount of LiBr encapsulated}}{\text{Total mass of capsules for analysing}} \times 100 \quad (2)$$

The EE and active load (AL) calculated for each capsule sample formed are enclosed in Table 1. The EE determined for the subsequent coatings is relative to the total amount of LiBr used in the formulation (silica capsules). There are several interesting points to note from the findings. The EE determined for the encapsulation of aqueous solution of LiBr to form silica capsules was very encouragingly 59 $\pm$ 3 %. However, there is a decrease in the EE determined after the following coatings and drops to 30 $\pm$ 2 % after the final polymer coating to form Si-NH_2-Au-NH_2 capsules. This loss in EE is most likely due to diffusion of LiBr through the capsule walls rather than weak capsules rupturing during the coating process as explained below.

Most interestingly, significant loss (24 %) in EE is observed after coating of the Au nanoparticles whereas, during the first polymer coating up to only 5 % is lost. Although all the capsules were exposed to similar physical and mechanical conditions such as stirring and temperature during each coating, approximately 5 times greater loss of EE is observed during the Au-nanoparticle coating compared to the APTMS coating, hence the most likely loss of LiBr is through diffusion and water ingress is most likely due to replace the loss LiBr, especially as the Au-nanoparticles coating was performed in aqueous media whereas the APTMS coating was carried out in PhMe. The solubility of LiBr in PhMe is poor and water is immiscible in PhMe. Therefore, diffusion into PhMe will be much slower compared to water. To evaluate whether this is the case, a release study of LiBr from the capsules over time in water was carried out over 2 h under the same conditions used for the Au nanoparticle coating. Figure 3 shows the release profile of LiBr from $SiNH_2$ capsules at room temperature. There is a burst of release from 0 to 1 h followed by slow release thereafter and at 2 h release of ~75 % is observed. Significant release of ~45 % is observed at 30 min immersion time,

which corresponds to the duration used for the Au nanoparticle coating. Even after 5 min of immersion time a release of ~15 % is observed.

Similarly to the EE, AL is the highest for the silica capsules which is observed as 15 ± 3 %, and it reduces subsequently after each step to 9 ± 3 % after the final polymer coating.

Table 1. Capsule size, shell thickness, EE and active load for the microcapsules.

Capsules	Microcapsule size (μm)			Mean Shell	EE (%)		Active load (%)	
	Size Range	Average	CV	Thickness (μm)	EE Range	EE Average	AL Range	AL Average
Silica	2.4-40.4	8.3	0.6	1.1 ± 0.2	55-61	59 ± 3	10-18	15 ± 3
$SiNH_2$	3.5-45.3	8.4	0.6	1.2 ± 0.2	53-57	54 ± 2	11-17	14 ± 3
$SiNH_2$-Au	3.0-46.8	9.0	0.7	1.5 ± 0.3	27-35	30 ± 4	5-12	10 ± 2
$SiNH_2$-Au-NH_2	3.1-45.2	9.2	0.7	1.5 ± 0.4	26-30	30 ± 2	5-12	9 ± 3

Note: the errors represent the standard errors associated with the measurement.

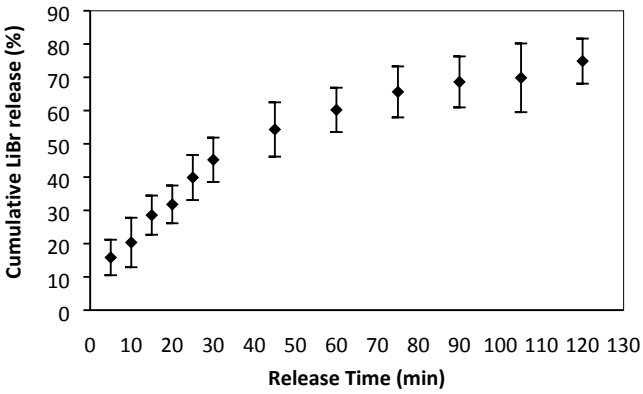

Figure 3. Cumulative LiBr release from Si-NH_2 over 2 h after immersion in water. The error bars represent the standard error associated with the measurement.

2.4 The success of the coating determined via zeta potential

The coating of the APTMS and citrate stabilised Au nanoparticles on the capsules alter the surface charge of the capsules, for instance, the silica coated capsules due to the presence of hydroxyl groups will be negatively charged whereas the presence of amine moieties from the successful coating of APTMS should lead to the surface becoming positively charged. Moreover, depending on the pH, the coating of the citrate stabilised Au nanoparticles should lead to negatively charged

capsules.[29,30] Hence, by measuring the zeta potential of the capsules, it should be possible to determine whether the coating of the multiple shells has been successful. However, the charge of the surfaces will be sensitive to the pH of medium as the pK_a of the functional groups present (-CO_2H or -NH_2) will determine whether the groups are protonated or deprotonated and thus whether the surface is charged (-CO_2^- or -$^+NH_3$) or neutral (-CO_2H or -NH_2).[29-31] The reported pK_a of aliphatic carboxylic acids is 4-5[32,33] and aliphatic secondary amine is 11 in free aqueous solution.[34,35] However, it is well documented that the pK_a of aliphatic acids and amine which are bound to a surface such as Au and silica substrate to form a self-assembled monolayer are different to what is observed in free solution.[36-43] It is postulated this is due to the combination of the potential of the surface influencing the pK_a and the closed packing of the molecules on the surface as the creation of charge on adjacent molecules which are in close proximity in the monolayer will culminate to unwanted repulsive forces being developed. Numerous studies have reported the pK_a of acid terminated monolayer to be higher than in free solution between 5-8[36-42] whereas for aliphatic amine it has been observed to be lower at 8.[43] As a consequence of the pH influencing the charge of the functional groups, zeta potential was measured over a pH range 3-10. The zeta potential measurements reported were taken at 25 ^oC at a concentration of 2 mg mL^{-1}. Each potential shown in Figure 4 is an average of three measurements taken on newly prepared sample at each pH, whose pH was modified via addition of 0.01 M NaOH and HCl aqueous solution. From Figure 4 it is evident that there is a change in the surface charge after each coating. As expected the surface on the silica coated capsules is negatively charged and the charge increases from -14 to 35 mV between pH range 3.5 to 5 and levels out with potential. It is envisaged to result from deprotonation of the -OH between 3.5 and 5 and saturation was reached after pH 5.

Interestingly, after the APTMS coating the charge on the capsule's changes to positive between pH 3.5-6 and then inverts to negative after pH 6.5, followed by a decrease in charge to -20 mV at pH 7 and remains relative constant thereafter. The presence of the positive charge between pH 3.5-6 suggests the presence of positive charge moieties on the surface of the capsules, and hence shows that there are amine moieties present on the capsule surface at high concentrations as they are having a greater influence on the surface charge than the -OH moieties. Moreover, there is a sudden change in zeta potential at pH 6.5, as the pK_a for amine functionalised self-assembled monolayer (SAM) is approached. It is postulated that the change of charge is a cause of the -OH groups dominating the charge of the capsules over the amine which will be mostly present as -NH_2.

In the case of the Au-nanoparticle coating there are several intriguingly points to note. The most evident observation from the plot is the surfaces are negatively charged over the pH range 3.5-10, which is in stark contrast to the APTMS coated capsules, hence this suggests that the negatively charged Au nanoparticles have successfully been deposited on the surface. Most interestingly there are two trends observed, one between pH 3.5-4.5 and the other trend after pH 4.5, which is unique for this coating in comparison to the other coatings. Initially from pH 3.5 to 4.5 the zeta potential decreases and reaches a minimum value of -32.7 ± 1.6 mV at pH 4.5. Thereafter, an increase is observed between pH 4.5-10 from -32.7 ± 1.6 mV to 12.5 ± 2.9 mV and interestingly, after pH 8 the zeta potentials are very similar to those observed for Si-NH_2 capsules. The trend observed is very interesting. As discussed earlier the reported pK_a of aliphatic -COOH and aliphatic secondary -NH_2 is 4-5[32,33] and 11,[34,35] respectively, hence it would be expected that the negative charge on the Au nanoparticles would increase with increasing pH due to the presence of -COOH moieties which will become more deprotonated with increasing pH and the underlying -NH_2 moieties will become less protonated as the pH increases. Therefore it would be envisaged that the zeta potential would decrease with increasing pH. Thus, the real mechanism of the observed increase in zeta potential after pH 4.5 needs to be further investigated in the future. Furthermore, interestingly, the pH at which the lowest zeta potential was observed (pH 4.5) is similar to the pH previously reported for optimum binding between the citrate stabilised Au nanoparticles and amine functionalised surface.[29.30]

The final coating of APTMS leads to positively charged surface in pH range of 3.5-6.0 followed by negative surface after pH 6.5 similarly to what was observed for the first coating of APTMS, although the magnitude of charge is smaller than what was observed after the initial coating of APTMS, which could be due to incomplete coverage. Overall this suggests the coating has been successful.

-

-

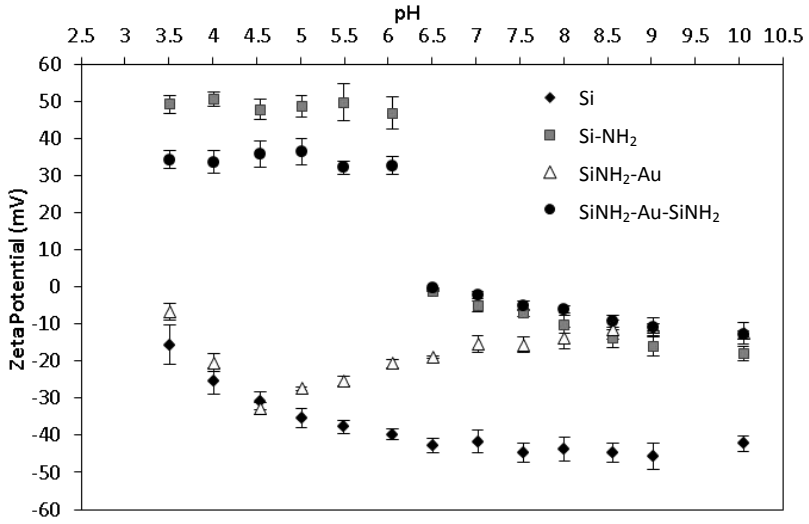

Figure 4. Zeta potential for the capsules as a function of pH.

2.5 Capsule DSC Thermograms

To evaluate the thermal stability of the capsules, as well as to observe any changes in the -temperature cycles indicative of the presence of the Au-nanoparticles on its surface, DSC thermograms were acquired for the $SiNH_2$-Au and the $SiNH_2$ capsules (Figure 5). To ensure the DSC thermograms were repeatable and hence show the capsules were chemically stable via the heating and cooling cycles, the capsules were continuously cycled 10 times from 25 to 150 ^oC and 150 to 25 ^oC and these are superimposed onto each other in Figure 5. First and foremost, it is evident from both curves that the first cycle is disparate to the follow up 9 isotherm curves, which are similar to each other. The first thermogram for $SiNH_2$ capsules has a broad peak within the temperature range 80 to 130 ^oC which is likely due to the water being removed from the capsules and any other contaminate which may have accumulated onto the capsules overtime. Interestingly, for Si-NH_2-Au capsules the peak is more sharply centred at 85 ^oC and is not as significant as observed for the Si-NH_2 capsules. Overall, the DSC thermal cycles show there is no evidence of chemical change over the 10 cycles apart from the removal of water and contaminates from the capsules in the first cycle and hence, which suggests the capsules are thermally stable over the temperature range (25 to 150 ^oC and vice versa). Furthermore, it is clearly evident that the Si-NH_2-Au capsules have a larger discrepancy between the heating and cooling curves in the DSC cycles i.e. larger area entrapped between the heating and cooling cycle; this is a result of the heat flow being more rapid in the initial stages of the heating and cooling curves, which suggests after Au nanoparticle coating, there was

change in physical properties of the tested material. This further provides evidence that there has been a chemical change in the material after the immersion of the capsules in colloidal suspension.

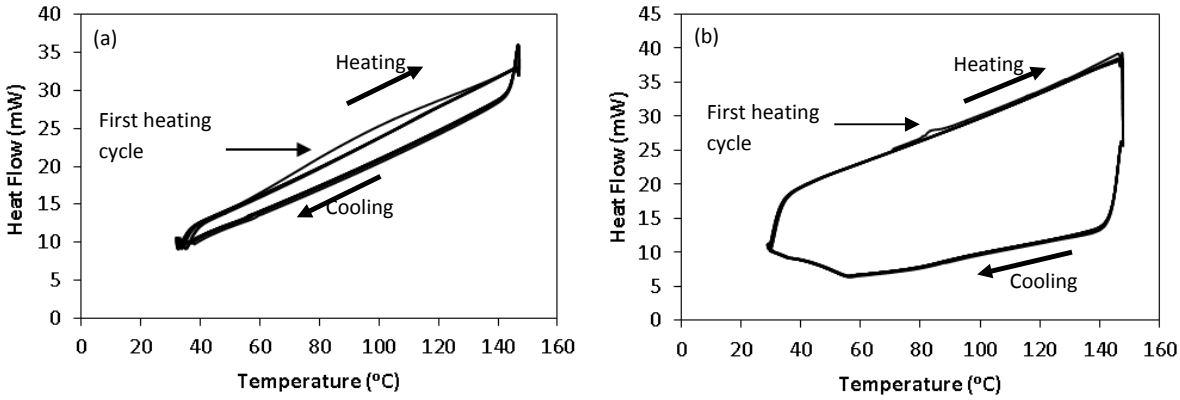

Figure 5. DSC thermograms for 10 continuous cycles for (a) $SiNH_2$ and (b) $SiNH_2$-Au capsules.

2.6 Mechanical properties before exposure to 10 thermal cycles

The mechanical properties of the capsules were tested using a micromanipulation technique,[44] where a glass capillary tube with small diameter of ~30 µm was used to crush the capsules with an aid of a force transducer (Max. scale 5mN, Model 403A, Aurora Scientific Inc., Canada). Table 2 shows the mechanical properties of the capsules prior and after exposing the capsules to 10 cycles of heating and cooling between temperatures -10 to 150 °C and vice versa.

Prior to heating, silica capsules have mean rupture force of 0.25 ± 0.02 mN, which is higher than what has been previously reported for similar silica capsules.[44] The rupture force does not increase significantly, after the coating with APTMS. However, after the coating with Au-nanoparticles the capsules become stronger with rupture force increasing by ~80 % to 0.45 ± 0.04 mN and deformation at rupture reduced by ~13 %. Hence, the capsules become stronger and more brittle with the Au nanoparticle coating. It was envisaged with significant coating of Au-nanoparticles, the surface would lose some of its underlying silica polymer's elastic properties but would be compensated with the increase in compressive strength, and therefore it seems the enhancement properties expected via the introduction of the Au nanoparticles has been accomplished. Again after the final APTMS coating there is no significant change in both deformation at rupture and rupture force by taking the standard error of the mean into consideration.

Table 2. Mechanical properties for capsules prior and after 10 repeated thermal cycles (-10 to 150 °C).

Capsules	Displacement at Rupture (µm)	Rupture Force (mN)	Deformation at Rupture (%)	Nominal Rupture Stress (MPa)
Silica	2.9 ± 0.4	0.25 ± 0.02	35 ± 3	4.6 ± 0.5
$SiNH_2$	3.2 ± 0.5	0.27 ± 0.03	37 ± 4	4.6 ± 0.6
$SiNH_2$-Au	1.9 ± 0.3	0.45 ± 0.04	22 ± 4	7.0 ± 0.7
$SiNH_2$-Au-NH_2	1.8 ± 0.2	0.47 ± 0.03	20 ± 2	7.0 ± 0.9
After Cycles				
Silica	2.4 ± 0.5	0.20 ± 0.05	29 ± 4	3.7 ± 0.6
$SiNH_2$	2.5 ± 0.5	0.20 ± 0.06	30 ± 4	3.6 ± 0.6
$SiNH_2$-Au	1.6 ± 0.4	0.32 ± 0.05	18 ± 4	5.0 ± 0.7
$SiNH_2$-Au-NH_2	1.4 ± 0.3	0.35 ± 0.04	15 ± 3	5.3 ± 0.9

Note: the error shown is the standard error associated with the measurement.

2.7 Capsules properties after exposure to 10 thermal cycles

To evaluate the capsules' suitability for the intended application as an alternative composite material to be used in cooling systems, the thermal stability of the capsules over the temperature range (-10 °C to 150 °C) which the capsules will be likely exposed to for the intended application needs to be investigated. Thus, the capsules were heated and cooled between the temperatures of -10 and 150°C in 10 repeated cycles, followed by characterisation using SEM, micromanipulation and flame photometry to determine changes in surface morphology, mechanical strength and LiBr retention. The characterisation was taken as soon as possible within 24 h to ensure the changes observed was due to the thermal cycles and not as a result of degradation overtime. Figure 6 shows the SEM images of the capsules after 10 thermal cycles. From the images there is no evidence of any changes in the capsules after the process. Most of the capsules remain intact without any degradation or rupture evident. The surface morphology remains similar without any clear change to the capsule surface, which suggests the capsules are stable. This is further supported by the EE and active load data calculated for the capsules after the process (Table 3). The discrepancy in EE and active load (Table 1) prior to and after the thermal cycles (Table 3) for all the capsules is insignificant. This suggests that the overwhelming majority of the silica coated capsules are stable to meet the thermal demands of the application. Moreover, there is no significant loss of LiBr from the capsules, hence virtually no water ingress has taken place due to no loss of LiBr. However, the determined average size for both the silica and coated silica capsules (NH_2, NH_2-Au and NH_2-Au-NH_2) after the exposure to the thermal cycles show a marginal decrease. Moreover, the CV for all the capsules after

the cycles is slightly lower than prior to heating, in fact the CVs are ~12-14 % lower than before the thermal cycles and it seems that the larger capsules have disappeared as the upper range in the size distribution is lower. For example for the silica capsules the size distribution prior to the cycles is 2.4-40.4 µm with CV 0.6 whereas after the size distribution is 2.5-30.4 µm with CV of 0.5. Thus, this suggests that the larger capsules may have ruptured during the thermal cycles. A little caution has to be taken on this finding as the variation may just be due to the larger capsules not being observed when calculating the size distribution after the thermal cycles. However, as the pattern is observed for all four capsules it is likely that this finding is a true reflection of the size distribution.

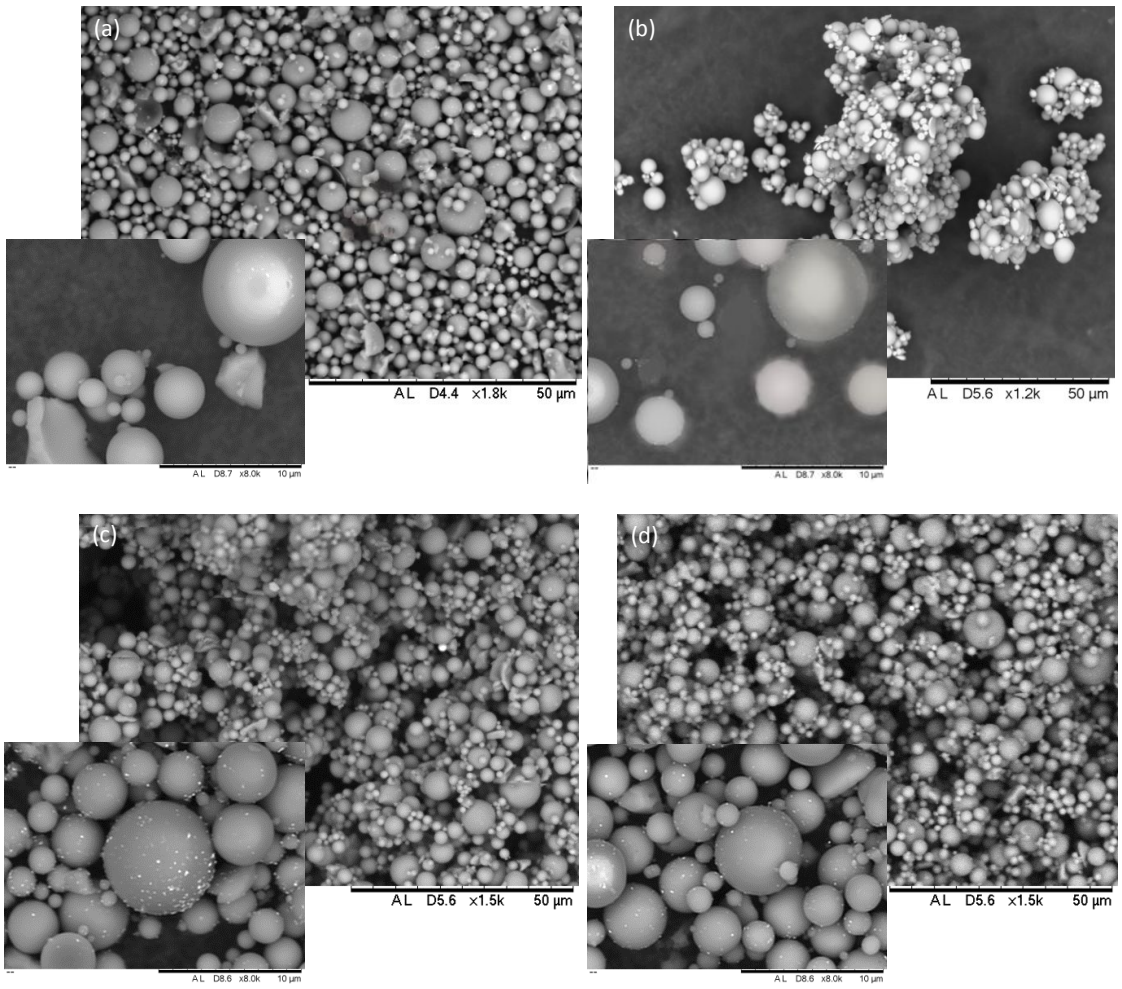

Figure 6. SEM images of the capsules after thermal exposure; (a) Silica, (b) $SiNH_2$ (c) $SiNH_2$-Au and (d) $SiNH_2$-Au-NH_2 microcapsules, insects show capsules with higher magnification.

Table 3. The capsule sizes, EE and active load for microcapsules after exposure to 10 repeated heating and cooling cycles between -10 to 150 °C.

Capsules	Microcapsule size (μm)			Encapsulation efficiency (%)		Active load (%)	
	Range	*Average*	*CV*	*Range*	*Average*	*Range*	*Average*
Silica	2.5-30.4	8.2	0.5	53-55	54 ± 1	8-17	13 ± 2
$SiNH_2$	3.6-39.3	8.3	0.5	50-53	51 ± 2	10-16	11 ± 3
$SiNH_2$-Au	3.0-35.8	9.0	0.6	29-35	30 ± 5	6-11	8 ± 2
$SiNH_2$-Au-NH_2	3.0-35.9	9.2	0.7	26-28	27 ± 1	4-11	8 ± 3

Note: the error shown is the standard error associated with the measurement.

2.7.1 Mechanical properties after exposure to 10 thermal cycles

After exposing the capsules to 10 repeated cycles of -10 to 150 °C, all the capsules have become more brittle with a 10-15% decrease in nominal deformation at rupture than prior to the cycles and this has led to a significant decrease in rupture force (20-30 %) for all the capsules (Table 2). To gain further understanding on whether the reduction in rupture force is continuously decreasing after each cycle, the rupture force was determined after exposing $SINH_2$-Au-NH_2 capsules to 2, 4, 6, 8 and 10 cycles. From Figure 7a, it can be observed that the rupture force decreases from 0.47 ± 0.07 mN to 0.35 ± 0.07 mN after cycle 6, and further decrease is not seen from cycle 6-10. Similar thread is observed in the displacement at rupture which decreases between cycles 0-6 from 1.8 ± 0.2 μm to 1.4 ± 0.3 μm and remains stable thereafter (Figure 7b). Furthermore, the nominal stress reduced from 7.0 ± 0.9 to 5.3 ± 0.9 MPa (Figure 7c). Hence, the capsules were mechanically weakened in the first 6 cycles and stabilised thereafter. The reduction in the mechanical properties of the capsules suggests that the capsule wall undergo degradation during the first 6 cycles which leads to weakening of the capsule walls. A plausible explanation for this finding could be related to the walls losing their elasticity during the first 6 cycles as the capsule walls expand and reform during the heating and cooling cycles, respectively. During the swelling the capsule walls become thinner and thus weaker and during the cooling cycle they should return to the original geometry. However, in this case it is postulated at the alleviated temperatures further polymerisation takes place between the remaining silanol moieties within the capsule walls which is catalysed by the H_2O from the capsule core leading to the walls becoming gradually more brittle and losing their elasticity and hence do not return to their original geometry when cooled to room temperature. So the capsule walls will be thinner than prior to heating and hence weaker, leading to lower rupture forces required. Furthermore, the increase in crossing linking between the silica moieties as a result of the polymerisation has led to the capsules becoming more brittle as shown by the decrease in displacement at rupture (Figure 7b). After 6 cycles it seems the polymerisation is fully saturated in

the capsule wall and thus, there is no further weakening of the capsule wall. Moreover, the further polymerisation during the heating cycles also explains the appearance of small amounts of agglomeration seen between the capsules, which were not observed prior to the cycles. This would suggest polymerisation is not only occurring within the capsule wall but also between the capsules, although at a smaller scale. Another plausible explanation for the observed decrease in the capsule wall's mechanical properties is related to the moisture content in the wall. If the moisture content in the capsule becomes less after each cycle until it reaches a plateau after cycle 6, this will lead to the internal pressure reducing after each cycle and the capsules becoming fewer firms which will subsequently lead to smaller rupture force required to break the capsule wall.

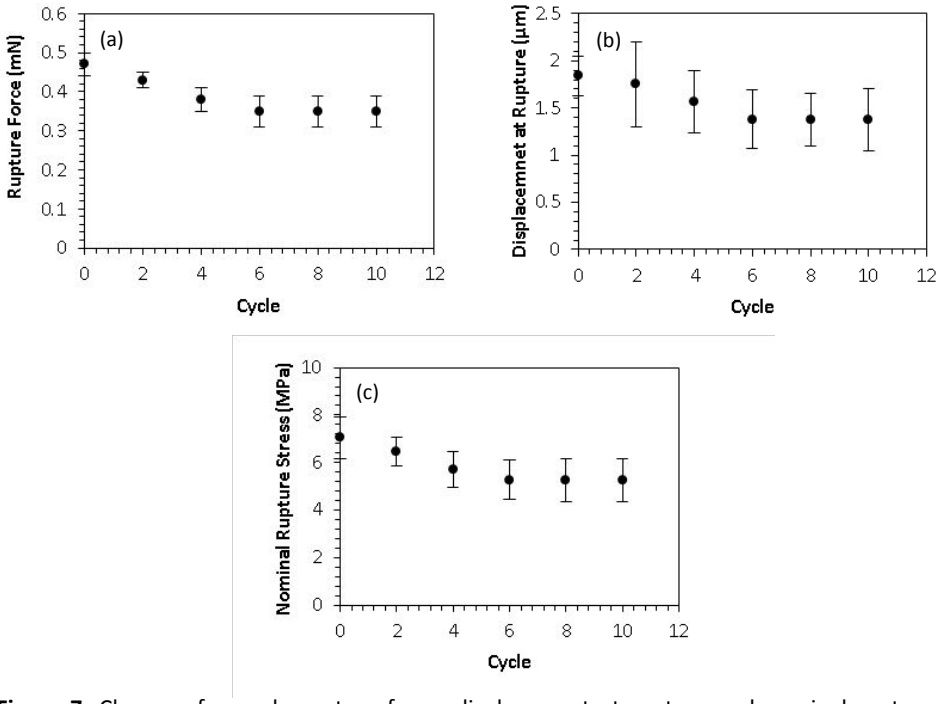

Figure 7. Change of capsule rupture force, displacement at rupture and nominal rupture stress as a function of number of thermal cycle.

To further explore the thermal effect on the capsule walls as well as investigate the plausibility of further polymerisation between the silanol moieties taking place, a study was performed to investigate the effect that the maximum temperature of the cycle has on the rupture force and displacement at rupture. If both parameters are temperature dependent this would further support a chemical reaction taking place within the capsule wall. Therefore, continuous 10 repeated cycles were performed from -10 ^{o}C to the maximum temperatures shown in Figure 8, followed by cooling to -10 ^{o}C. From Figure 8a and 8b, a reduction is observed in both parameters with increasing

temperature from -10 to 150 °C, suggesting the capsules are becoming more brittle and weaker which correlates with the earlier findings. The plots suggest a linear relationship between the capsule rupture force and displacement at rupture versus temperature, which suggests that a chemical reaction is taking place within the capsule walls. Interestingly, as expected increasing the temperature accelerates the polymerisation within the capsule wall leading to weaker and more brittle walls.

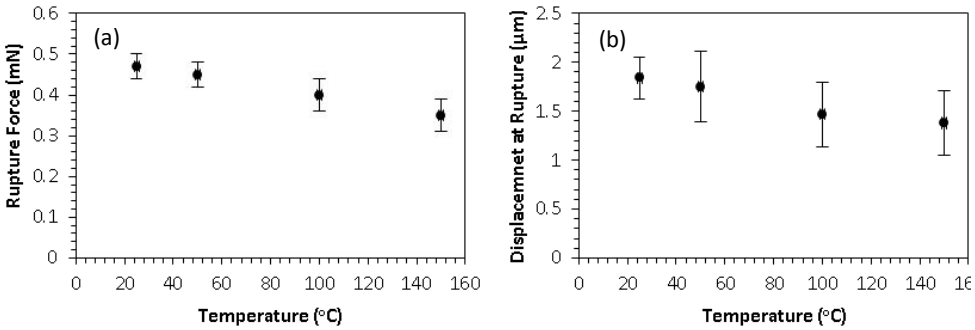

Figure 8. The change of (a) rupture force and (b) displacement at rupture as a function of temperature after 10 thermal cycles.

2.8 Adsorption-Desorption Cycles

To preliminarily evaluate the adsorption and desorption of water from the capsules, a purpose built rig was constructed (see ESI, Figure S5), which contained a jacketed casing comprised of two co-axial tubes. The rig was packed with the capsules and repeatedly heated and cooled continuously between the temperatures -14 to 150 °C for 10 cycles. Figure 9 shows the changes in the pressure during the desorption (heating, pressure increase) and adsorption (cooling, pressure decrease) cycles observed for the capsules. There are several interesting findings from the plot: first and foremost, the adsorption and desorption cycles are similar and repeatable over the 10 cycles. The pressure constantly rises to ~450000 Nm^{-2} during the desorption, which is repeatable from cycles 5-10. This suggests that the water vapour is successfully adsorbed and desorbed over the 10 cycles and hence no water loss. Most importantly as each cycle is relatively identical in terms of shape, this suggests the capsules are stable and have not undergone any chemical or physical change during the thermal heating and cooling process. This observation is further supported by the SEM images of the capsules after exposure to the thermal cycles in the rig (Figure 10a). The capsules maintain their quasi-spherical shape and the surface morphology is similar to prior to the cycles (Figure 1d). Moreover, there is no evidence of capsules rupturing, however there is slight evidence of minimal

coalescence between the capsules similar to what was previously observed after the thermal cycles in DSC (Figure 10b), which was not evident prior to the cycles. It is envisaged this is likely as a result of cross chain polymerization of unreacted silane during the thermal cycles between the capsules.

Interestingly, it is clearly evident that the maximum pressure is not obtained after the first cycle but on the fifth cycle and remains relatively similar thereafter indicating the optimum water release from the capsules has been reached. This suggests the water is strongly held within the capsules and takes several cycles for the water to be released as a consequence of the presence of high concentration of LiBr in the capsules. The efficiency in releasing water could be improved via maintaining the temperature at 150 °C for longer time. In fact, it is evident from Figure 10, when the temperature is maintained at or slightly increases around 150 °C for 10 min, an obvious increase in pressure is observed in all of the 10 cycles. This could be attributed to the resistance of capsule shell to the water vapor; it takes a while for the gas to penetrate the capsule wall. Moreover, lower concentration of LiBr could be used, this should lead to the water being released more efficiently however this will compensate the water adsorption ability of the capsules. Overall, the preliminary adsorption and desorption cycles show the capsules are efficient towards adsorbing and desorbing water, although further work needs to be undertaken to optimize the system.

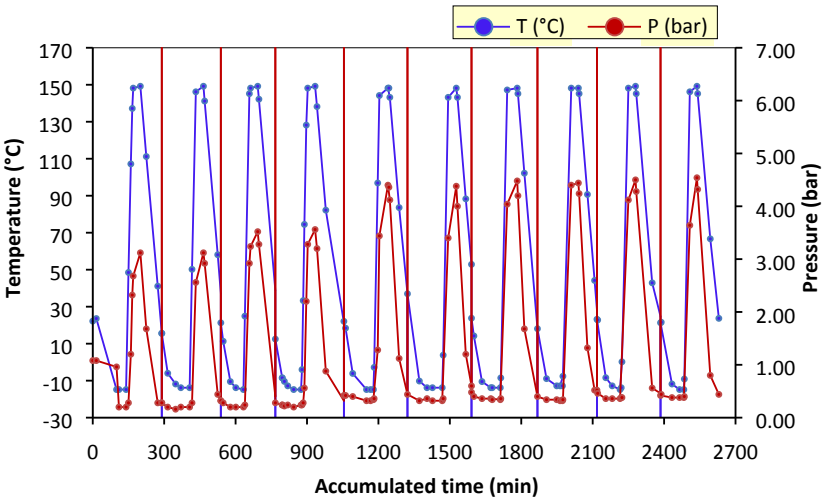

Figure 9. Continuous 10 adsorption and desorption cycles performed on the capsules in a custom made rig.

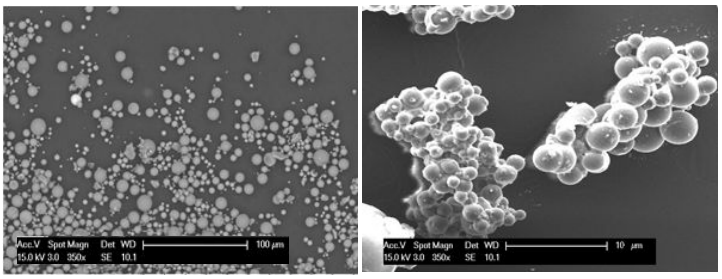

Figure 10. SEM images of capsules after 10 adsorption and desorption cycles in the rig.

3.0 Experimental

3.1 Material and methods

Commercially available chemicals were purchased from Sigma Aldrich and solvents from Fisher Scientific or VWR and used as received.

3.1.1 Preparation of silica coated capsules via in-situ polymerisation. First and foremost the silica precondensate was synthesised. A mixture of teraetoxysilane (TEOS), methyltrimethoxysilane (MTMS) and water (1:1:1.3 eq) was heated to 100 ^{o}C and kept for 4.5 h to form precondensate followed by stirring at room temperature for 16 h. The MTMS was added to introduce hydrophobicity on the capsule surface so to prevent agglomeration from happening between the capsules during and after the preparation of the capsules.

A 62 % (w/w) solution of lithium bromide in 0.1 $HCl_{(aq)}$(1 g) was added dropwise to a stirred mixture of mineral oil (75 g), silica precondensate (6.4 g) and silica nanoparticles (18 nm, 0.1 g) using an IKA turbine Mixer homogeniser. The resultant emulsion was stirred for 15 minutes at room temperature followed by further stirring at 50 ^{o}C for 1 h. After 1 h, MTMS (3 g) was added dropwise (to ensure capsule shell completion and to prevent capsule agglomeration) and the resulted mixture stirred for a further 1 h at 50 ^{o}C. The reaction mixture was then allowed to cool to room temperature (22 ± 1 ^{o}C) and the microcapsules were collected by suction filtration and washed thoroughly with hexane to obtain a white powder (2.15 g).

3.1.2 Amine functionalisation of silica coated LiBr capsules. Silica capsules (300 mg) were added to anhydrous toluene (25 mL). The resulted suspension was stirred for 10 min at room temperature

under $N_{2(g)}$ atmosphere to ensure the removal of aggregates of microcapsules followed by addition of APTMS (3 ml) dissolved in PhMe and the reaction mixture was stirred overnight at room temperature under $N_{2(g)}$ atmosphere. The microcapsules were collected by suction filtration and washed thoroughly with PhMe (3 x 25 ml) to obtain white capsules (300 mg).

3.1.3 Synthesis of citrate stabilised Au nanoparticles. A solution of $HAuCl_4.3H_2O$ (40 mg) in Ultra High Quality (UHQ) H_2O (49 mL) was heated under reflux for 10 min followed by addition of a solution of sodium citrate (80 mg) in UHQ H_2O (1 mL). The resultant solution was heated under reflux until colour change was observed from yellow to red wine at which point the solution was further refluxed for 5 min to ensure complete reduction of the gold salt. The colloidal suspension was cooled to room temperature. The cooled colloidal suspension was centrifuged at 3500 rpm with a centrifugal force equivalent to 235 N for 10 min and the supernatant was collected. The centrifugation was repeated twice to remove any gold aggregates. Finally, the pH of the colloidal suspension was adjusted to 4.5 by addition of 0.06 M HCl.

3.1.4 Formation of Au nanoparticle bilayer on amine functionalised silica capsules. Amine functionalised silica capsules (100 mg) were added to citrate stabilised Au colloidal suspension (5 mL) followed by sonication for 3 min. The resulted suspension was further stirred at room temperature for 27 min. The capsules were collected by suction filtration and washed with UHQ H_2O to give purplish white powder (80 mg).

3.1.5 Formation of silica coated layer on Au nanoparticle coated capsules. Similar procedure was followed as described for amine functionalisation of the silica capsules in section 3.1.2.

Au nanoparticle coated capsules (50 mg) were added to anhydrous PhMe (5 mL). The resulted suspension was stirred for 10 min at room temperature under $N_{2(g)}$ atmosphere to ensure the removal of aggregates of microcapsules followed by addition of APTMS (7.5 µL) and the reaction mixture was stirred overnight at room temperature under $N_{2(g)}$ atmosphere. The microcapsules were collected by suction filtration and washed thoroughly with PhMe to obtain purplish white powder (40 mg).

3.2 Capsule characterisation

3.2.1 Encapsulation efficiency (EE) and active Load. To determine the EE for the capsules, the respective capsules (50 mg) were ground in UHQ H_2O (2.5 ml) using a mortal and pistol for 1 min and left standing for 1 h with periodical thorough grinding every 15 min over the 1 h. The ground

mixtures were filtered (0.45 μm) and the samples were further diluted tenfold with UHQ H_2O to produce 10 mL samples. LiBr content was then analysed using a Corning 400 flame photometer by determining the Li^+ ions concentration in the prepared solutions with calibration curve of known Li^+ ion concentration solutions. Triplicate experiments were undertaken for each capsule and the errors given for each measurement is the standard error.

3.2.2 Capsule shell thickness. Liquid nitrogen was poured onto the capsules followed by crushing the capsules using pistol and mortar for 1 min. SEM samples were prepared as described in section 3.2.7.

3.2.3 UV-vis spectroscopy. The UV/Vis spectra were obtained using a Varian Cary 50 UV0902M053 UV-Visible spectrophotometer and samples were analysed using a 1 cm length of quartz cuvette.

3.2.4 Dynamic Light Scattering (DLS). The microcapsule sizes were determined using a Particle Analyzer (DelsaTM Nano Submicron Particle Size and Zeta Potential) equipped with a laser He-Ne (3.0 mW, 633 nm) and photodiode detector. The results were analysed using DelsaTM Nano UI software version 3.73. All the measurements were performed in H_2O in a 1 cm path length quartz cell at 25 ^oC. The temperature was controlled by a thermo-electric Peltier heater/cooler element. A time lapse of 1 min was set between the sample being placed in the DLS chamber and the measurement being performed to ensure the samples equilibrated to 25 ^oC prior to the measurement being taken. Average measurements reported were taken from 10 measurement cycles for each type of microcapsules and the error given is the standard error.

3.2.5 Zeta potentiometry. As described for the DLS measurements, microcapsules (20 mg) were dispersed in the UHQ H_2O (2 ml), the resultant suspension was sonicated for 5 min. The pH was adjusted to the required pH with aliquot addition (10 μl) of 0.05 M $HCl_{(aq)}$ and 0.05 M $NaOH_{(aq)}$. The resultant suspension was further sonicated for 5 min prior to the measurement being performed. The process was repeated two more times for each pH and capsule coating.

3.2.6 Differential Scanning Calorimetry (DSC). DSC was performed on a DSC7 Perkin-Elmer machine using Al crucibles. The temperature was increased with a heating rate of 10 $^oC\ min^{-1}$ from 25 to 150 ^oC, then consolidated at 150 ^oC for 5 min, followed by decrease in temperature from 150 to 25 ^oC at a rate of 10 $^oC\ min^{-1}$, and then consolidation at 25 ^oC for 5 min. This cycle was further repeated 9 times for each microcapsule sample.

3.2.7 Scanning Electron Microscopy (SEM). Microcapsules were distributed evenly on a SEM stub which was sputtered coated with 5 nm thick Au or carbon film (to visualise the Au nanoparticles). The samples were imaged using either benchtop Hitachi TM3030 SEM or XL series Philips XL30 FEG

ESEM with electrical voltage 15 kV.

3.2.8 Transmission Electron Microscopy (TEM). The images of the citrate stabilised Au nanoparticles were observed using a JEOL JEM-1200EX and a JEOL JEM-2100 electron microscope fitted with a Gatan camera. Two samples of TEM Formvar/carbon film-coated Cu-grids with 200 mesh (Ager Scientific) were prepared by applying one drop (10 μL) of the particle suspension on each grid and they were left to be dried in air for 24 h.

3.2.9 Flame Photometry. A Corning 400 flame photometer with max pressure 0.21 kg cm^{-2} was used to determine the Li^+ ions concentration in the prepared solutions. A calibration curve was prepared using known Li^+ ion concentration solutions; 1, 2, 3, 4, 5, 6, 7, 8, 9, 10, 20, 30, 40, 50, 60, 80, 90 and 100 ppm. Depending on the strength of the Li^+ ion concentration in the samples either standard 10 or 100 ppm Li^+ ion solution was used as the upper limit on the Flame photometer i.e. for a solution with a weaker Li+ ion concentration than 10 ppm the Flame photometer upper limit was set at 10 ppm and 100 ppm if greater than 10 ppm. H_2O was used as the blank. Each sample was run three times to ensure same readings were obtained each time.

3.2.10 Micromanipulation. Droplets from a diluted suspension of the capsules in hexane (1 mg/mL) were placed on glass slides and left to air dry for 2 h. In the case of the capsules which underwent thermal cycles, the capsules were cooled before being dispersed in hexane. The glass slide was placed on the stage of a micromanipulation rig to perform the compressions. Single microcapsules were compressed between two flat surfaces. Force transducer (Model 403A Aurora Scientific, Inc., Canada) was used with a glass mounted probe with diameter of 20 μm and 80 μm to compress the microcapsules of 4-40 μm in diameter, at a compression speed of 2 μm s^{-1}. 25 capsules were analysed for each data set in order to generate statistically representative results and the error stated is the calculated standard error. A typical force versus displacement curve for compression of single microcapsules to rupture is shown in ESI (Figure S3) with definitions of the rupture force, displacement at rupture, nominal deformation at rupture and nominal rupture stress.

3.2.11 **Adsorption-Desorption Cycles.** The Adsorption-Desorption cycles were performed on a purpose built column containing a test jacketed casing which consists of two coaxial tubes: one has 1 inch OD and another has ¾ inch OD. A refrigerated/heating circulator was equipped for duo purpose of heating/cooling the thermal liquid as well as pumping it upwards through the jacket to heat/cool the inner tube and the tested capsules which were packed in the inner tube. As the temperature changes, the capsules adsorb or desorb the water accordingly which subsequently leads to variation of the pressure inside the tube. The pre-weighed capsules were charged into the inner tube with the

assistance of tapping the tube to remove any voids and to obtain an even packed bed. After closing both the inlet and outlet valves, the refrigerated/heating circulator and the pump were switched on to enable the cold thermal liquid to pass through the annular space of the jacket until the lowest set temperature was reached (-14 ^{o}C). The system was maintained at this temperature for 10 min prior to initiating the vacuuming of the system. The outlet valve was opened after starting the vacuum pump. When the pressure was stable and further reduction was not observed over 5 min, the outlet valve was closed. The system was then isolated and ready for testing. Initially, the system was heated at the full power of the heater at a rate of 7 °C/min to 150 ^{o}C via the refrigerated/heating circulator. The temperature was maintained at the highest temperature for 10 min. After which the system was cooled to -14 ^{o}C at a rate of 2 ^{o}C min^{-1} and maintained at -14 ^{o}C for further 10 min, followed by repetition of the heating and cooling cycles for further 9 cycles. During all these cycles the temperature and pressure were recorded periodically i.e. 3-5 readings were taken during the heating and cooling cycles as well as during the periods when constant temperature was maintained.

4.0 Conclusions

This work successfully demonstrated the encapsulation of aqueous LiBr solution, forming capsules with average size less than 10 µm, good encapsulation efficiency and active load. Further functionalization of the capsules via coating with APTMS followed by coating with Au nanoparticles and finally APTMS coating have shown to be successful via data obtained from zeta potential, SEM and mechanical properties. The coating of Au nanoparticles has enhanced the mechanical properties of the capsules. However, a significant amount of LiBr salt was lost during the coating with the Au nanoparticles. Further work needs to be performed to improve the encapsulation efficiency.

Moreover, the capsules were shown to be thermally stable after exposing them to heating and cooling cycles from -10 to 150 ^{o}C and vice versa and there was no significant change in the encapsulation efficiency and active load. However, the mechanical properties of all the capsules were affected leading to weaker and more brittle capsule walls. The structural morphology of the capsule remains intact, although there is evidence of minimal amount of agglomeration between the capsules. Most importantly, preliminary adsorption and desorption cycles on the capsules are encouraging and show the pressure output remains constant over the 10 cycles.

5.0 Acknowledgements

The authors would like to acknowledge ESPRC for providing financial support [EP/W021142/1] to the work described in this paper. We would also like to thank Professor Jon A. Preece in the School of Chemistry at University of Birmingham for giving us access to his facilities. We acknowledge Birmingham Science City; Innovative Uses for Advanced Materials in the Modern World (West Midlands Centre for Advanced Materials Project 2), which is funded by Advantage West Midlands (AWM) and the European Regional Development Fund (ERDF) for access to their instruments as well as Birmingham Centre for Energy Storage at University of Birmingham.

6.0 Supporting Information.

Information on the characterisation of the Au nanoparticles, size distribution of the capsules prepared, SEM images of shell thickness as well as a typical force versus displacement curve for compression of a single silica capsule is included. Moreover, a description on how the Au nanoparticle surface coverage on each capsule was calculated is found within the supporting information.

7.0 References

1. Mitchell SW. On the use of Bromide of Lithium. *Am J Med Sci.* **1870**, *60*, 443.
2. Shorter, E, The history of Lithium Therapy, Bipolar Disord. 2009, 11, 4.
3. Owens, D. C. Chapter 11: Clinical Pyschopharmacology, Companion to Psychiatric Studies, *8th Edition*, Elserver Ltd, **2010**, 266.
4. Hasaninejada, A.; Zareb, A.; Mohammadizadeha, M. R.; Shekouhy M. Lithium Bromide as an Efficient, Green, and Inexpensive Catalyst for the Synthesis of Quinoxaline Derivatives at Room Temperature. Green Chemistry Letters and Reviews **2010**, *3*, 143.
5. Saini, A.; Sandu, J. S. LiBr: A Mild Lewis Acid Catalyst for Efficient One-Pot Synthesis of Alpha-Amino Nitriles. *Chem. Commun*. **2008**, *38*, 3655.
6. Sasson, Y.; Weiss, M.; Loupy, A.; Bram, G.; Pardo, C. Bromide-Chloride Exchange Between Alkyl Halides and Metal Halide Salts under Phase Transfer Conditions. *J. Chem. Soc., Chem. Commun.* **1986**, 1250.
7. Ingold, K. U.; Walton, J. C. Cycloalkylmethyl Radicals. 5. 6- to 15-Membered Rings: ESR Studies of Ring Conformations and Stereodynamics. *J. Am. Chem. Soc.* **1987**, *109*, 6937.
8. Gordeeva, L. G.; Restuccia, G.; Cacciola G.; Aristov, Y. I. Selective Water Sorbents for Multiple Applications, 5. LiBr Confined in Mesopores of Silica Gel: Sorption Properties. *React. Kinet. Catal. Lett.* **1998**, *63*, 81.
9. Pandya, B.; Kumar, V.; J. Patel, J; Matawala, V. Optimum Heat Source Temperature and Performance Comparison of LiCl-H_2O and LiBr-H_2O Type Solar Cooling System. *J. Energy Resour. Technol.* **2018**, *140*, 051204.
10. Srikhirin, P.; Aphomratana, S.; Chungpaibulpatana, S. A Review of Absorption Refrigeration Technologies. *Renewable Sustainable Energy Rev.* **2001**, *5*, 343.
11. X. Wang, X.; Chua, H. T. Absorption Cooling: A Review of Lithium Bromide-Water Chiller Technologies. *Recent Patents on Mech. Eng.* **2009***, 2,* 193.
12. Arshi Bano, P.S.; Sudharsan, N. M. Review of Water Based Vapour Absorption Cooling Systems Using Thermodynamic Analysis. *Renewable Sustainable Energy Rev.* **2018**, *82*, 3750.
13. Gilani, S. I.; Ahmed, M. S. M. S.; Solution Crystallization Detection for Double-Effect LiBr-H_2O Steam Absorption Chiller. *Energy Procedia* **2015**, *75*, 1522.
14. Vericella, J. J.; Baker, S. E.; Stolaroff, J. K.; Duoss, E. B.; Hardin, J. O.; Lewicki, J.; Glogowski, E.; Floyd, W. C.; Valdez, C. A.; Smith, W. L.; Satcher Jr., J. H.; Bourcier, W. L.; Spadaccini, C. M.; Lewis J. A.; Aines, R. D. Encapsulated Liquid Sorbents for Carbon Dioxide Capture. *Nat. Commun*. **2015**, *6*, 6124.
15. Dubey, R.; Shami T. C.; Bhasker Rao, K. U. Microencapsulation Technology and Applications. *Defence Sci. J*., **2009**, *59*, 82.

16. Jyothi, N. V. N.; Prasanna, P. M.; Sakarkar, S. N.; Prabha, K. S.; Ramaiah P. S.; Srawan, G. Y. Microencapsulation Techniques, Factors influencing Encapsulation Efficiency. *J. Microencapsulation,* **2010**, *27*, 187.

17. Srls, J.; Seethadevi, A.; Prabia, K. S.; Muthprasanna P.; Pavitra, P. Microencapsulation: A Review. *International J. Pharma and Biosciences,* **2012**, *3*, 509.

18. Chevalier Y.; Bolzinger, M.-A. Emulsions Stabilized with Solid Nanoparticles: Pickering Emulsions. *Colloids and Surfaces A: Physicochem. Eng. Aspects* **2013**, *439*, 23.

19. Kumpugdee-Vollrath, M; Tabatabaeifar, M.; Helmis, M. New Coating Materials Based On Mixtures of Shellac and Pectin for Pharmaceutical Products *Engineering and Technology, International Journal of Medical, Pharmaceutical Science and Engineering* **2014**, *8*, 26.

20. Do, T.; Ko, Y. G.; Chun, Y.; Choi, U. S. Encapsulation of Phase Change Material with Water-Absorbable Shell for Thermal Energy Storage. *ACS Sustainable Chem. Eng.* **2015**, *3*, 2874.

21. Zhu, Y.; Liang, S.; Wang, H.; Zhang, K.; Jia, X.; Tian, C.; Zhou, Y.; Wang, J. Morphological Control and Thermal Properties of Nanoencapsulated n-Octadecane Phase Change Material with Organosilica Shell Materials. *Energy Convers. Manage.* **2016**, *119*, 151.

22. Chang, T. M.; Semipermeable Microcapsules. *Science* **1964**, *146*, 524.

23. Hitchcock, J. P.; Tasker, A. L.; Baxter, E. A.; Biggs, S.; Cayre, O. J. Long-Term Retention of Small, Volatile Molecular Species within Metallic Microcapsules. *ACS Appl. Mater. Interfaces* **2015**, *7*, 14808.

24. Patchan, M. W.; Baird, L. M.; Rhim, Y.-R.; Y.-R. LaBarre, Y.-R.; Maisano, J.; Deacon, R. M.; Xia, Z.; Benkoski, J. J. Liquid-filled Metal Microcapsules. *ACS Appl. Mater. Interfaces* **2012**, *4*, 2406.

25. Sahlot, M.; Riffat, S. B. Desiccant Cooling Systems: A Review. *International J. Low-Carbon Technol.* **2016**, *11*, 489.

26. Renz, M.; SteimLe, F. Thermodynamic Properties of the Binary System, Methanol-Lithium Bromide. *Int. J. Refrig.* **1981**, *4*, 97.

27. Mendes, P.; Belloni, M.; Ashworth, M.; Hardy, C.; Nikitin, K.; Fitzmaurice, D.; Critchley, K.; Evans S.; Preece, J. A. A Novel Example of X-Ray-Radiation-Induced Chemical Reduction of an Aromatic Nitro-Group-Containing Thin Film on SiO_2 to an Aromatic Amine Film. *ChemPhysChem* **2003**, *4*, 884.

28. Du, Y.; Li, L.; Leung, C. W.; Lai, P. T.; Pong, P. W. T. Synthesis and Characterization of Silica-Encapsulated Iron Oxide Nanoparticles. *IEEE Trans. Magn.* **2014**, *50*, 1.

29. Diegoli, S.; Mendes, P. M.; Baguley, E. R.; Leigh, S. J.; Iqbal, P.; Garcia Diaz, Y. R.; Begum, S.; Critchley, K., Hammond, G. D.; Evans, S. D.; Attwood, D.; Jones, I. P.; Preece, J. A. pH-Dependent Gold Nanoparticle Self-Organization on Functionalized Si/SiO_2 Surfaces. *J. Exp. Nanosci.,* **2006**, *1*, 333.

30. HamLett, C. A. E.; Docker, P. T.; Ward, M. C. L.; Prewett , P. D.; Critchley, K.; Evans, S. D.; Preece, J. A. pH-Dependent Adsorption of Au Nanoparticles on Chemically Modified Si_3N_4 MEMS devices. *J. Exp. Nanosci.* **2009**, *4*, 147.

31. Coradin, T.; Mercey, E.; Lisnard, L; Livage, J; Design of Silica-coated Microcapsules for Bioencapsulation. *Chem. Commun*. **2001**, 2496.

32. Iqbal, P.; Critchley, K.; Bowen, J.; Attwood, D.; Tunnicliffe, D.; Evans, S. D.; Preece, J. A. Fabrication of a Nanoparticle Gradient Substrate by Thermochemical Manipulation of an Ester Functionalized SAM. *J. Mater. Chem.* **2007**, *17*, 5097.

33. pK_a of ethanoic acid is given as 4.75 in Atkins, P. W. *Physical Chemistry, 6th edition*, Oxford University Press, Oxford, UK, **1998**, 933.

34. pK_a of ethanoic acid is given as 4.76 in Stewart, R. *The Proton: Applications to Organic Chemistry*, Academic Press, Orlando, Canada, **1985**, 24.

35. pK_a of tertiary amine is given as ~10.65 in Patai, S. *The Chemistry of the Amino Group*, Interscience Publishers, London, UK, 1968, 174.

36. pK_a of tertiary amine is given as ~10.7 in Solomons, T. W. G. *Organic Chemistry, 6th Edition*, John Wiley & Sons, New York, USA, 1996, 902.

37. Lee, T. R.; Carey, R. I.; Biebuyck, H. A.; Whitesides, G. M. The Wetting of Monolayer Films Exposing Ionizable Acids and Bases. *Langmuir* **1994**, *10*, 741.

38. Godínez, L. A.; Castro, R.; Kaifer, A. E. Adsorption of Viologen-Based Polyelectrolytes on Carboxylate-Terminated Self-Assembled Monolayers. *Langmuir* **1996**, *12*, 5087.

39. Hu, K.; Bard, A. J. Use of Atomic Force Microscopy for the Study of Surface Acid−Base Properties of Carboxylic Acid-Terminated Self-Assembled Monolayers, *Langmuir* **1997**, *13*, 5114.

40. White, H. S.; Peterson, J. D.; Cui, Q.; Stevenson, K. J. Voltammetric Measurement of Interfacial Acid/Base Reactions. *J. Phys. Chem. B* **1998**, *102*, 2930.

41. Kokkoli, E.; Zukoski, C. F. Surface Forces between Hydrophilic Self-Assembled Monolayers in Aqueous Electrolytes, *Langmuir* **2000**, *16*, 6029.

42. Sugihara, K.; Shimazu, K. Electrode Potential Effect on the Surface pKa of a Self-Assembled 15-Mercaptohexadecanoic Acid Monolayer on a Gold/Quartz Crystal Microbalance Electrode. *Langmuir* **2000**, *16*, 7101.

43. Schweiss, R.; Welzel, P. B.; Werner, C.; Knoll, W. Dissociation of Surface Functional Groups and Preferential Adsorption of Ions on Self-Assembled Monolayers Assessed by Streaming Potential and Streaming Current. *Langmuir* **2001**, *17*, 4304.

44. Wang, B.; Oleschuk, R. D.; Horton, J. H. Chemical Force Titrations of Amine- and Sulfonic Acid-Modified Poly(dimethylsiloxane), *Langmuir* **2005**, *21*, 1290.

45. Mercadé-Prieto, R.; Allen, R.; Zhang, Z.; York, D.; J. A. Preece, J. A.; Goodwin, T. E. Failure of Elastic-Plastic Core–Shell Microcapsules Under Compression. *Particle Technology and Fluidization* **2012**, *58*, 2674.

TOC Graphic

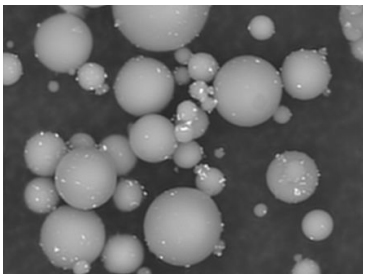

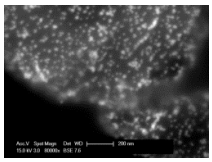

Capsule surface coated with Au nanoparticles.